Navigating the chaos of psychedelic fMRI brain-entropy via multi-metric evaluations of acute psilocybin effects

Drummond E-Wen McCulloch[1,2,†], Anders Stevnhoved Olsen[1,3,†], Brice Ozenne[1,4], Dea Siggaard Stenbæk[1,5], Sophia Armand[1,5], Martin Korsbak Madsen[1,6], Gitte Moos Knudsen[1,7], Patrick MacDonald Fisher[1,8]

[1]Neurobiology Research Unit, Copenhagen University Hospital, Rigshospitalet, Copenhagen, Denmark

[2]Faculty of Health and Medical Sciences, University of Copenhagen, Denmark

[3]Department of Applied Mathematics and Computer Science, Technical University of Denmark, Kgs. Lyngby, Denmark

[4]Section of Biostatistics, Department of Public Health, University of Copenhagen, Copenhagen, Denmark

[5]Department of Psychology, University of Copenhagen, Denmark

[6]Department of Psychiatry Svendborg, Svendborg, Denmark

[7]Department of Clinical Medicine, University of Copenhagen, Copenhagen, Denmark

[8]Department of Drug Design and Pharmacology, University of Copenhagen, Copenhagen, Denmark

[†]These authors contributed equally to this work

Abstract

A prominent theory of psychedelics is that they increase brain entropy. Twelve studies have evaluated psychedelic effects on fMRI brain entropy quantifications, no findings have been replicated. Here we evaluated these metrics in an independent 28-participant healthy cohort with 121 pre- and post-psilocybin fMRI scans. We assessed relations between brain entropy and plasma psilocin, brain serotonin 2A receptor occupancy, and a subjective drug intensity rating using linear mixed-effects models. We observed significant positive associations for Shannon entropy of path-length, instantaneous correlation distributions, and divergent associations of sample entropy at varying time-scales. We did not observe significant effects for 8 of 13 entropy metrics. Brain entropy quantifications showed limited inter-measure correlations. Our observations support a nuanced acute psychedelic effect on brain entropy, underscoring the need for replication and that these metrics do not reflect a singular construct. Our findings highlight candidate brain entropy metrics that may mediate clinical effects of psychedelics.

Introduction

Psychedelic drugs induce profound altered states of consciousness including affective, sensory and cognitive effects mediated by activation of downstream pathways initiated by agonism at the brain serotonin 2A receptor [1–4]. In combination with psychological support, clinical studies up to phase 2b indicate promising clinical efficacy of psychedelics in the treatment of affective and behavioural neuropsychiatric disorders that may be associated with their acute effects [5–10,10–12]. Similarly, psychedelics induce acute and lasting effects on behaviour and personality in healthy participants [13–15]. In parallel to evaluating clinical treatment effects, human brain functional magnetic resonance imaging (fMRI) has begun to shed light on neural pathways affected by psychedelics [16].

Several prominent theories of critically relevant psychedelic effects on brain function have been advanced [17]. A prominent theory is the "Entropic Brain Hypothesis" (EBH), which posits that the 'richness' of the phenomenology of the acute psychedelic state reflects brain-wide increases in entropy of functional brain signals [18,19]. The concept of "entropy" serves as a quantification of the degree of information or complexity contained in a system; it is typically expressed in bits, without physical dimensions. Entropy has been conceptualised as a metric of information content and is largely defined in terms of a probability distribution; the metric is commonly referred to by the eponymous name "Shannon entropy" $H(X) = -\sum_{x \in X} p(x) \cdot log_2 p(x)$ where H(X) refers to the Shannon entropy of probability mass function X containing bins (x) with height (p) [20]. Other entropy metrics have been defined, e.g., Lempel-Ziv complexity and sample entropy [21–24], and adapted to characterise information contained in various objects, e.g., complex networks or graph structures [25].

To date, 12 studies have evaluated either acute or lasting psychedelic effects on the information-entropy of brain-activity or connectivity using blood oxygen level dependent (BOLD) fMRI data (Figure 1), one of which evaluates two metrics, thus 13 entropy metrics have been previously evaluated in this field. Four papers analysed data from a study evaluating 2mg intravenous psilocybin administration in up to 15 healthy participants [19,26–28]. Two papers reported effects from a study evaluating 75µg intravenous LSD administration in 15 healthy participants [29,30]. Two papers evaluated data from both datasets [31,32]. Three papers reported effects from a study evaluating oral ayahuasca administration, containing 96-160mg DMT and 25.2-42mg harmine (a monoamine oxidase inhibitor that facilitated the oral bioavailability of DMT) in 9 healthy participants [33–35]. Finally, one paper reported effects from a study evaluating lasting effects of 25mg/70kg bodyweight orally administered psilocybin in 11 healthy participants [36]. Notably, and highlighted in a recent review [16], each of these reports quantified a distinctly different metric of brain entropy. Here we group these metrics into three categories: 1) "static connectivity", 2) "dynamic connectivity", i.e., the time-varying relation between two or more time-series, 3) "dynamic activity", i.e., the entropy of regional time-series (Figure 1). Nine of these metrics are based on the Shannon entropy of distributions, three are Lempel-Ziv complexity metrics of a time-series and one is the sample entropy of a time-series. Taken together, although there is a clear interest in evaluating psychedelic effects on brain entropy, prominent limitations include that none of these measures have been evaluated in an independent cohort, the set of effects have been evaluated in only a few datasets, some with atypical modes of drug administration, and the inter-correlation between these metrics has not been considered. Previous studies compared pre-drug or placebo and a single post-drug scan. For the most part, these previous studies report increased brain entropy with only a few exceptions, e.g., two studies report non-significant psilocybin

effects and one study reports no lasting changes (Figure 1, Table 1). See Supplementary Table S1 for more details about the previous studies. Previous fMRI studies have reported reduced brain entropy in other states of "reduced consciousness", including NREM sleep [37], minimal-consciousness [38], and anaesthesia [39], whereas other studies have shown increased brain entropy following caffeine [40] and Salvinorin A intake [41].

In the current study, we sought to evaluate the acute effects of 0.2-0.3mg/kg psilocybin administration on these 13 brain entropy metrics in an independent dataset of 28 healthy individuals. Based on the entropic brain hypothesis, we hypothesised that brain entropy metrics would be increased following psilocybin administration. Participants completed a 5 or 10-min resting-state fMRI scan a single time before, and multiple times following psilocybin administration (121 total scan sessions). All scans for each participant were performed on one of two scanners. Each scan was accompanied by a self-report measure of subjective drug intensity (SDI) and a blood sample to quantify plasma psilocin level (PPL), from which brain serotonin 2A (5-HT2A) receptor occupancy (Occ_{2A}), was estimated based on its relation to PPL established in a previous study from our lab [2]. We evaluated the relations between each entropy metric and SDI, PPL and Occ_{2A} using linear mixed-effect model with a subject-specific random intercept and correction for age, sex, scanner, and motion (see Methods Supplementary Material for more details). We report uncorrected permutation p-values (p_{perm}) for each metric producing a single whole-brain value. For entropy metrics producing regional values, we report family-wise error rate corrected permutation p-values (p_{FWER}) with correction across all regions within each metric using maxT correction [42]. We report as significant those metrics which were significantly (i.e., $p < 0.05$) associated with SDI, PPL and Occ_{2A}, collectively referred to as “PsiFx”. Standardised effect sizes are reported (Pearson’s rho). This evaluation was repeated across two parcellation strategies and seven pre-processing pipelines to explore the robustness of effects to pre-processing decisions. Finally, we explored the inter-correlation between brain entropy metrics to characterise their associations.

Dynamic Activity

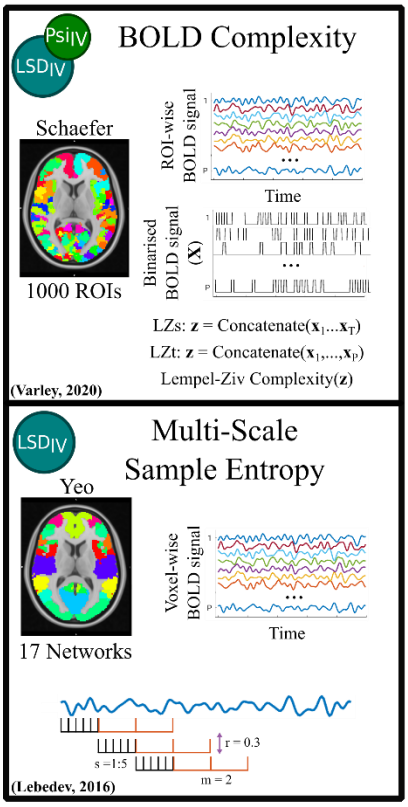

Static Connectivity

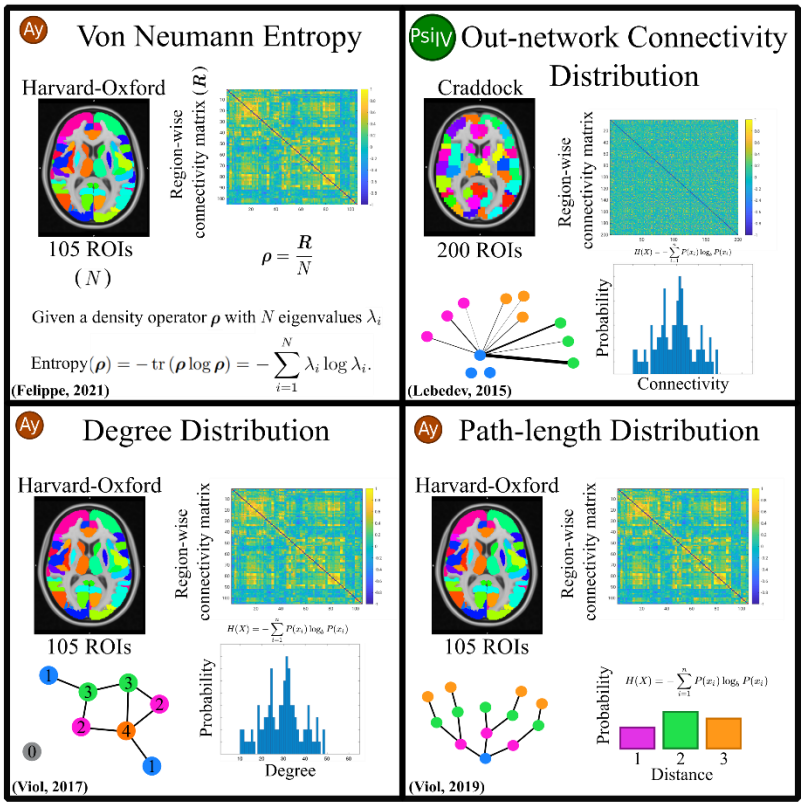

Dynamic Connectivity

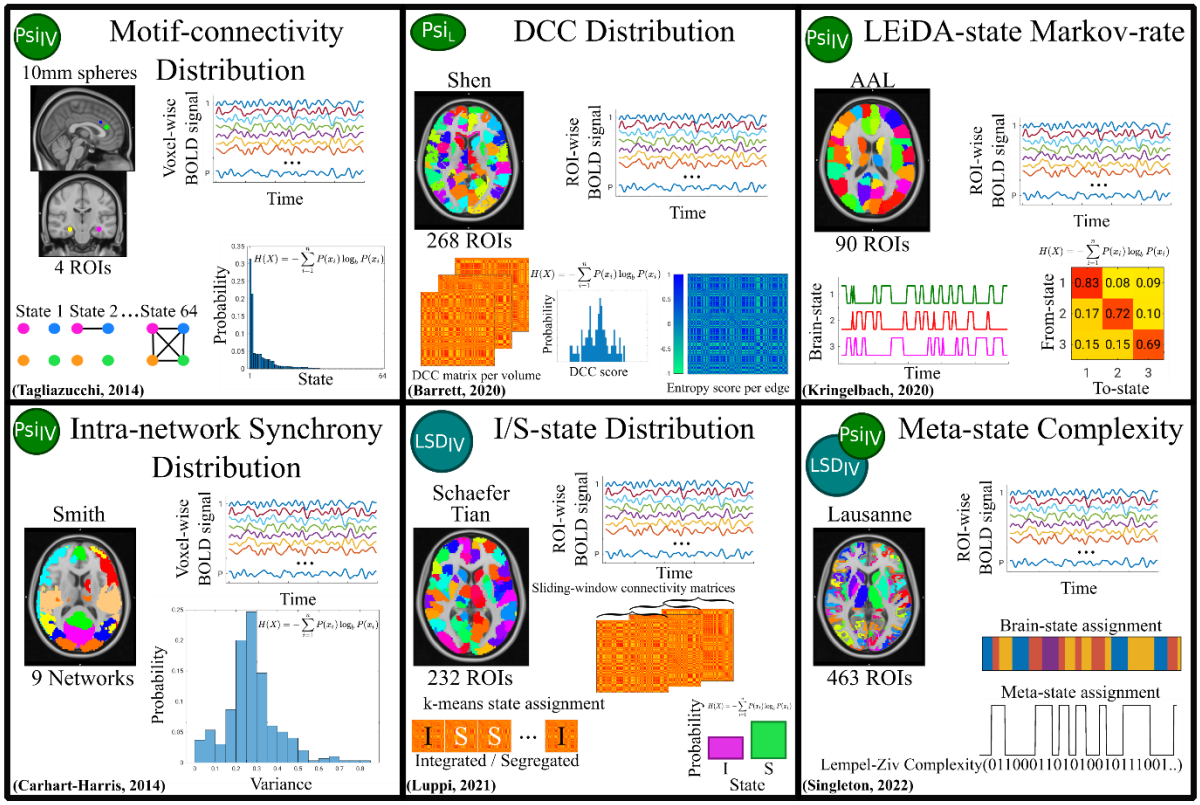

Figure 1: Overview of previous psychedelic fMRI entropy quantifications. Methods are grouped according to the type of brain entropy metric. Symbols in the top left of each box represent the dataset that the original publication analysed. LSD_{IV} (blue) refers to data collected in relation to a 75 µg intravenous LSD administration (n <= 15), Psi_{IV} (green) refers to data collected in relation to a 2 mg intravenous psilocybin administration (n <= 15), Ay (orange) refers to data collected in relation to an oral ayahuasca administration (n = 9), and Psi_{L} (green oval) refers to data collected one-week before, one-week after, and one-month after a 25 mg/70 kg oral psilocybin administration (n = 11). Brain images show an axial slice illustrating the parcellation/atlas used. Images in the top right describe the input into the entropy function as one of "region-wise connectivity matrix", "ROI-wise BOLD signal" and "voxel-wise BOLD signal". Illustrations in the lower part of each box graphically represent simplified analysis steps for each method. The original publication for each metric is denoted in the bottom left corner of each box. See Supplementary Table 1 for more details.

Results

Participants showed substantial SDI and PPL following drug administration as anticipated (Supplementary Figure S1). See Figure 1, Supplementary Table S1 and Table 1 for a summary of entropy metrics, previous findings, and our findings respectively.

Entropy of Static Connectivity

Out-network Connectivity Distribution

Shannon entropy of regional out-network connectivity was not significantly associated with psilocybin effects (PsiFx) in any of the 181 non-cerebellar brain regions after controlling for multiple comparisons ($p_{FWER} > 0.07$ for all regions for at least one of PsiFx, Supplementary Table S2).

Degree Distribution

The entropy of degree distribution at a correlation coefficient threshold corresponding to a mean degree of 27 was not associated with any of PsiFx ($p_{perm} > 0.18$, Figure 2A). We also did not observe significant effects for thresholds producing a mean degree between 1 and 48 (Supplementary Table S3).

Path-length Distribution

The entropy of path-length distribution was significantly positively associated with PsiFx at the a priori described threshold producing mean degree 27 ($p_{perm} < 0.04$, Figure 2B). The associations were weak to moderate (Pearson's rho = 0.39, 0.27, and 0.23 for PPL, Occ_{2A} and SDI, respectively). Significant weak to moderate positive associations with PsiFx were also observed across thresholds producing mean degrees from 22 to 38 (Supplementary Table S3).

Von Neumann Entropy

The Von Neumann entropy of correlation matrices was not significantly associated with PsiFx ($p_{perm} > 0.35$, Figure 2C and Supplementary Table S3).

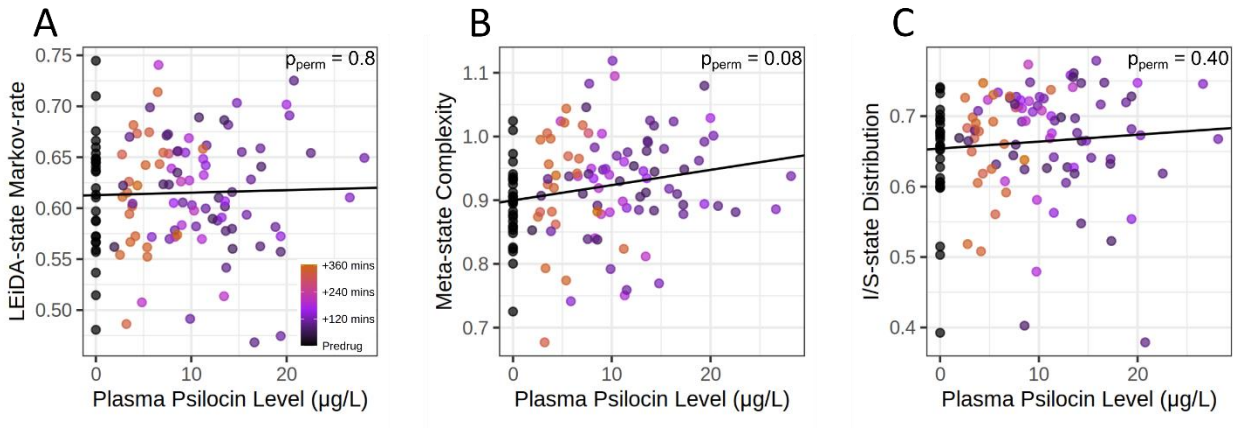

Figure 2: Scatter plots describing the relation between static connectivity entropy and PPL. Y-axis values are partial residuals i.e., entropy values adjusted for age, sex, MR scanner and motion. Degree distribution and path-length distribution statistics are computed using a correlation coefficient threshold corresponding to a mean-degree of 27.

Entropy of Dynamic Connectivity

Intra-network Synchrony Distribution

Intra-network synchrony distribution was not significantly associated with PsiFx in any of nine networks (All $p_{FWER} > 0.98$, Supplementary Table S2, Supplementary Figure S2).

Motif-connectivity Distribution

The four-ROI motif-connectivity state distribution was not significantly associated with PsiFx at any window length from 15 to 150s except a single weak association at window-length 100s ($p_{perm} < 0.05$, Pearson's rho 0.30, 0.25, and 0.24 for PPL, Occ_{2A}, and SDI, respectively) surrounded by non-significant findings (Supplementary Figure S3 and Supplementary Table S3).

LEiDA-state Markov-rate

LEiDA-state Markov-rate was not significantly associated with PsiFx ($p_{perm} > 0.7$ for all PsiFx, Figure 3A, Supplementary Table S3).

Meta-state Complexity

Meta-state entropy was positively associated with Occ_{2A} (p_{perm} = 0.03) and SDI (p_{perm} = 0.003), but not PPL (p_{perm} = 0.076, Figure 3B). Associations were weak (Pearson's rho = 0.22, 0.33, and 0.20 for Occ_{2A}, SDI, and PPL, respectively; Supplementary Table S3).

Integration/Segregation-state Distribution

Integration sub-state entropy was not significantly associated with PsiFx (p_{perm} > 0.06 for all PsiFx, Figure 3C, Supplementary Table S3).

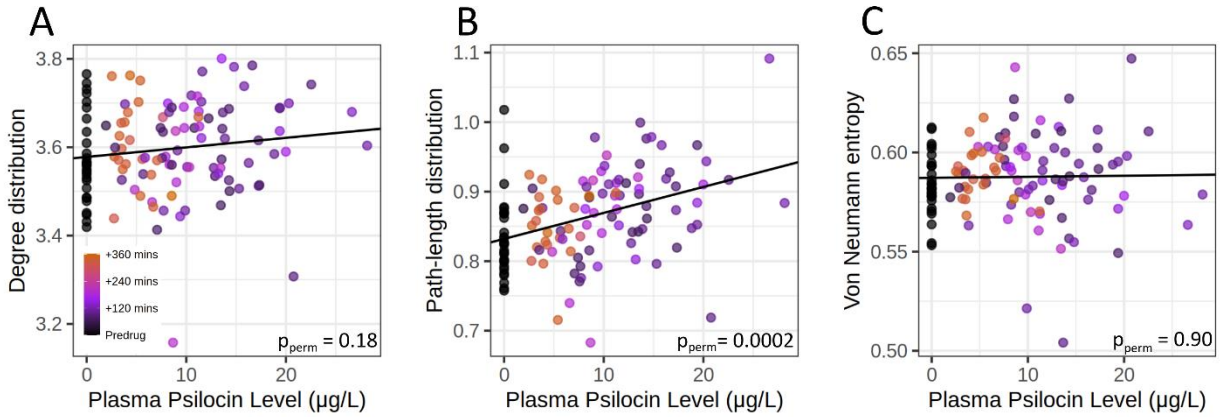

Figure 3: Scatter plots and linear models describing the relation between whole-brain dynamic connectivity entropy measures and plasma psilocin levels. Y-axis values are partial residuals i.e., entropy values adjusted for age, sex, MR scanner and motion. Panel B (Meta-state complexity) shows a non-significant association with PPL but this entropy metric does show a significant linear relation with Occ_{2A} and SDI.

Dynamic Conditional Correlation Distribution

Dynamic conditional correlation entropy was significantly positively associated with PsiFx in 35 of 36 network-network connections (18/36 p_{FWER} < 0.0001, i.e., observed data superseded all permutations, 29/36 p_{FWER} < 0.001, 35/36 p_{FWER} < 0.05; Figure 4A; Supplementary Table S2). Associations were moderate to strong (Pearson's rho range: 0.35 to 0.78, Supplementary Table S2). The one association with at least one non-significant relation was for edges within the motor cortex.

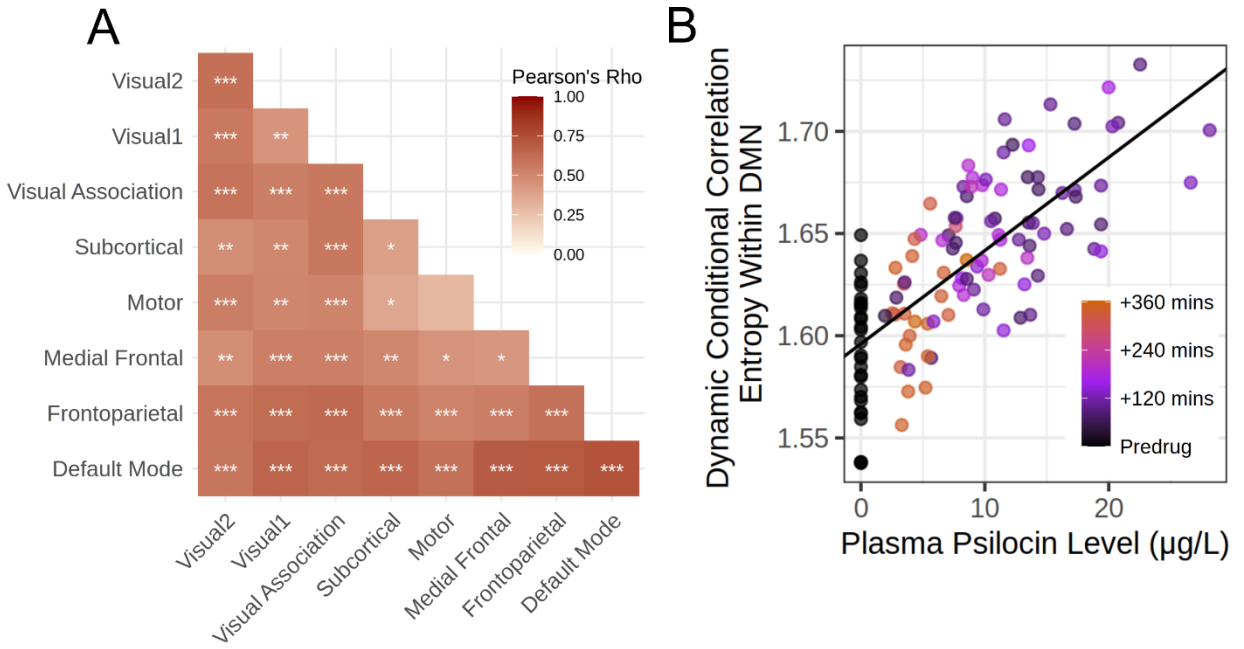

Figure 4: A: Heatmap of the Pearson's correlation and p-values for the association between Dynamic Conditional Correlation entropy and plasma psilocin level for each within and between network entropy estimate. *** represents $p_{FWER} < 0.0001$, ** $p_{FWER} < 0.001$, and * $p_{FWER} < 0.05$ for associations with PPL. **B:** A scatter plot of the network edge with the strongest association between DCC entropy and PPL (Pearson's Rho = 0.74). Y-axis values are partial residuals i.e., entropy values adjusted for age, sex, MR scanner and motion.

Entropy of Dynamic Activity

Multi-Scale Sample Entropy

At scale 1, (i.e., no time-series compression), sample entropy was significantly positively associated with PsiFx ($p_{FWER} < 0.05$) in 7 of 17 networks (i.e., Central Visual, Dorsal Attention A, Control A, B and C, Default-Mode A and C). At scales 2, 3, and 4, no associations were significantly associated with PsiFx ($p_{FWER} > 0.05$). At scale 5, sample entropy was significantly negatively associated with PsiFx in 14 of 17 networks; Control A and C and Default-Mode A ($p_{FWER} < 0.001$), Somatomotor A, Dorsal Attention A and B, Salience-Ventral-Attention B, Limbic B, Control B, Temporal-Parietal, Default-Mode B and C ($p_{FWER} < 0.05$, Figure 5, Supplementary Table S2). Scale 1 associations were weak to moderate (Pearson's rho range: 0.26 to 0.47), as were Scale 5 associations (Pearson's rho range: -0.27 to -0.49).

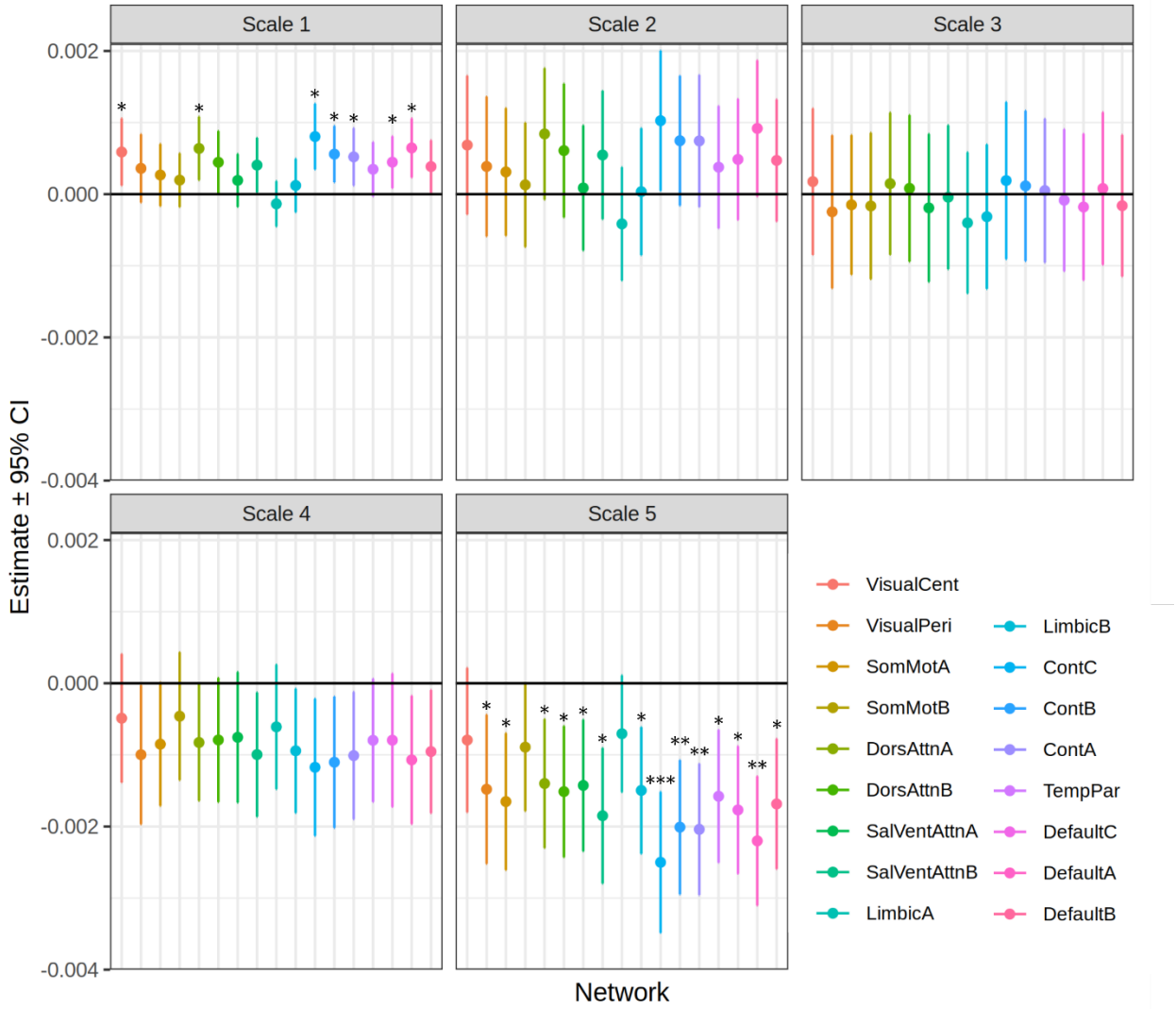

Figure 5: Forest plots representing the estimate of the association between sample entropy and PPL in each network of the Yeo-17 network parcellation and at each of scales 1 to 5. Colours represent networks and error bars represent the 95% confidence interval. *** $p_{FWER} < 0.0001$, ** $p_{FWER} < 0.001$ and * $p_{FWER} < 0.05$ for associations with PPL.

Spatial and Temporal Dynamic BOLD Complexity

Temporal BOLD complexity (LZct) was not associated with PPL (p_{perm} = 0.14, Figure 6B) but was associated with Occ_{2A} (p_{perm} = 0.03) and SDI (p_{perm} = 0.009). Associations were weak (Pearson's rho = 0.23, 0.30 and 0.17 for Occ_{2A}, SDI, and PPL respectively). Spatial BOLD complexity (LZcs) was not significantly associated with PsiFx (p_{perm} > 0.6, Figure 6A, Supplementary Table S3).

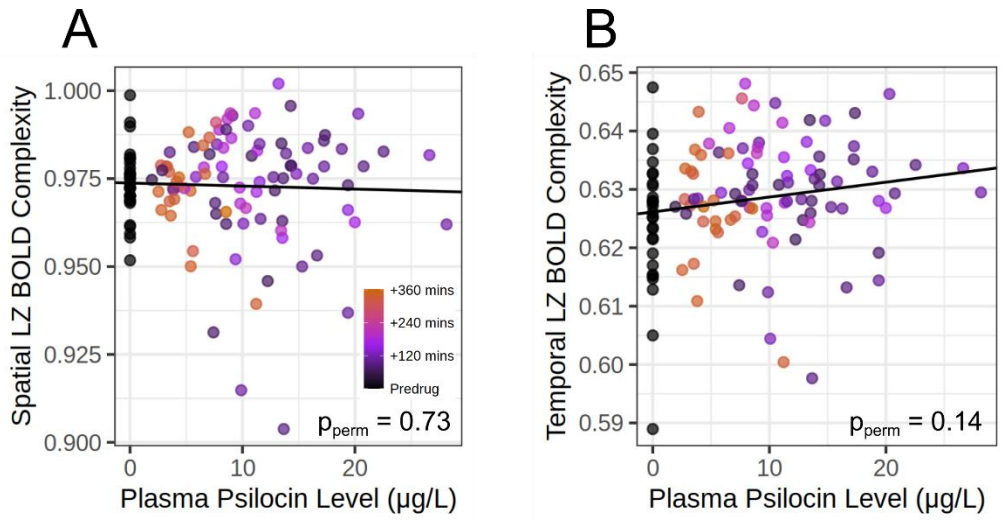

Figure 6: Scatter plots and linear models describing the relation between spatial (A) and temporal (B) Lempel-Ziv entropy of dynamic BOLD activity and PPL. Y-axis values are partial residuals i.e., entropy values adjusted for age, sex, MR scanner and motion. Temporal BOLD complexity (LZct) was significantly, but weakly associated with both Occ_{2A} and SDI despite not being significantly associated with PPL.

Effect of Parcellation

To evaluate PsiFx on brain entropy metrics using a common parcellation, all analyses were re-run using an atlas combining the Schaefer-100 (7 Yeo networks) and Tian-16 subcortical atlases[43,44]. Path-length distribution showed a weak positive association with all PsiFx at mean degrees 31 to 38. Meta-state complexity was weakly positively associated with Occ, but not PPL nor SDI. LEiDA-state Markov-rate was weakly negatively associated with all PsiFx and DCC distribution was weak-to-strongly associated with all PsiFx across most network edges. Sample Entropy was weak-to-moderately associated with PsiFx at scale 1 but no significant associations were observed at longer scales, though the trend of increased entropy at short scales and decreased entropy at long-scales was maintained. All other metrics were not significantly associated with PsiFx. See Table 1 for a summary and Supplementary Table S5 for detailed results.

Effect of Pre-processing Pipeline

To explore moderating effects of pre-processing pipelines on PsiFx associations with brain entropy metrics, we considered six variations on the above Schaefer-100, Yeo-7, Tian-16 pipeline: 1) including global-signal regression, 2) removal of the low-pass filter (0.09 Hz), 3) applying a narrow bandpass filter (0.03-0.07 Hz), 4) regressing 24 motion parameters, 5) omitting scrubbing, and 6) a stricter scrubbing threshold ($z > 3$ SDs, motion > 0.5mm). Some brain entropy metrics were relatively robust to pre-processing pipeline, i.e., showing significant associations with PsiFx across most pipelines: sample entropy (scale 1), dynamic conditional correlation entropy, meta-state complexity and path-length distribution. Some metrics were consistently not associated with PsiFx across pipelines: motif-connectivity distribution, I/S state distribution, LEiDA-state distribution and Intra-network synchrony. Some metrics were significantly associated with PsiFx for some pipelines and not others: temporal BOLD complexity (i.e., only significant with no-scrubbing and strict scrubbing) and Von Neuman Entropy (i.e., only significant with GSR and significant associated with SDI and Occ_{2A} when the low-pass filter was removed). Two pre-processing pipelines modulating signal-filtering had substantial effects on results. First, removing the low-pass filter flipped the sign to negative for the association between PsiFx and dynamic conditional correlation entropy and sample entropy (scale 1). Second, a narrow-band filter (0.03-0.07 Hz) made non-significant all PsiFx associations with dynamic and dynamic-connectivity metrics. See Supplementary Table S8 for a summary and Supplementary Table S9 for a full detailing of pre-processing effects.

Moderating Effect of Scanner

To evaluate scanner effects on observed associations, we fit linear mixed models estimating the moderating effect of scanner. Of the three entropy metrics that had a significant association with PsiFx, we observed a significant moderating effect of scanner on the relation between PPL and entropy for path-length distribution over the range of thresholds at which we observe significant associations with PsiFx. The nature of this interaction was that for scanner A the effect was closer to zero than for scanner B. We also show a significant moderating effect of scanner for Sample Entropy scale 5 across many ROIs that are significantly associated with PsiFx. However, the observed effect is the same direction for scanner A and B, only numerically stronger for scanner A. We do not observe a significant moderating effect of scanner for DCC entropy, further supporting the robustness of this metric. For entropy metrics that were not associated with PsiFx in the main model, we observed moderating effects of scanner for I/S-state distribution, some window-lengths of motif-connectivity distribution, some ROIs of out-network connectivity, degree distribution, and some sample entropy scale 4 ROIs. See Supplementary Table S6 for full results.

Correlation Between Whole-brain Entropy Quantifications

We estimated the correlation between whole-brain entropy metrics to explore their association with one another across all included scans. Some pairs of metrics were both positively correlated and negatively correlated and some pairs were effectively not correlated with one another (Figure 7). After correction for multiple comparisons, five entropy quantification pairs were positively related (LZcs & LZct, LZcs & Von-Neumann, Path-distribution & Degree-distribution, LEiDA state & Von-Neumann, Motif Connectivity Distribution-window100 & Von-Neumann) and four were negatively related (Path-distribution & LEiDA state, Path-distribution & Von-Neumann, Degree-distribution & LEiDA state, Degree-distribution & Von-

Neumann). LZcs was significantly negatively associated with motion. See Supplementary Table S4 for pairwise correlation coefficients and p-values.

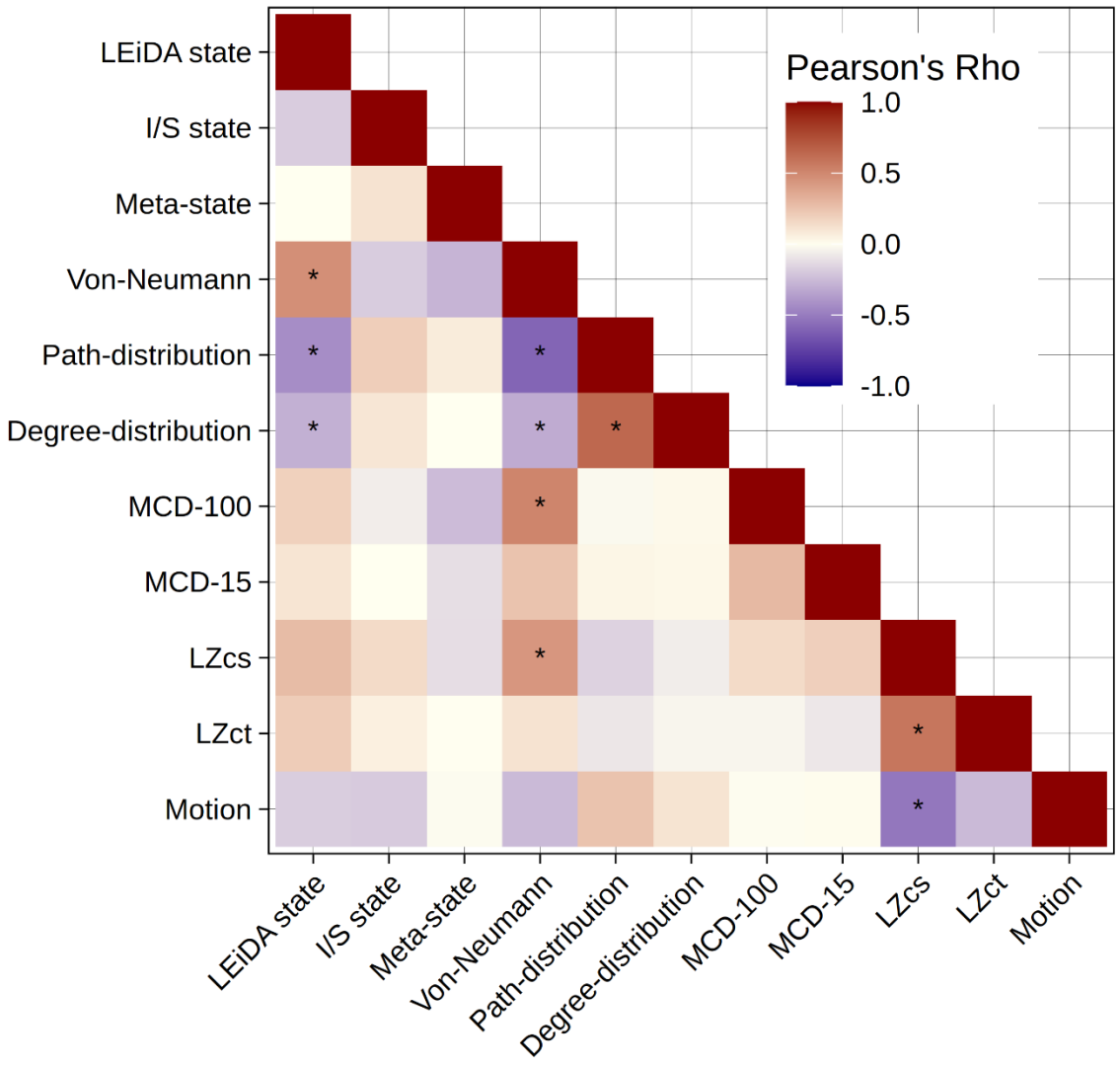

Figure 7: Heatmap showing the correlations between whole-brain entropy metrics and motion. Colours represent the Pearson's correlation coefficient. * represents $p_{corr} < 0.05$. I/S state, Integration/Segregation state distribution; MCD, Motif connectivity distribution (with either 100 or 15 second windows); LZcs, Spatial Lempel-Ziv complexity. LZct, Temporal Lempel-Ziv complexity.

Entropy	Original dataset	Original findings	Our findings (original atlases)	Our findings (common atlas)
Static Connectivity				
Out-network connectivity	IV Psi	Region-specific effects	Not associated with PsiFx	Not associated with PsiFx
Degree distribution	Oral Aya	Increased	Not associated with PsiFx	Not associated with PsiFx
Path-length distribution	Oral Aya	Increased	Weak-moderate association with PsiFx†	Weak-moderate association with PsiFx‡
Von Neumann Entropy	Oral Aya	Numerically increased	Not associated with PsiFx	Not associated with PsiFx
Dynamic Connectivity				
Intra-network synchrony	IV Psi	Increased (some networks)	Not associated with PsiFx	Not associated with PsiFx
Motif-connectivity distribution	IV Psi	Increased	Not associated with PsiFx	Not atlas dependent
Meta-state complexity	IV Psi & IV LSD	No change	Weak association with SDI and Occ but not PPL	Weak association with Occ but not SDI or PPL
I/S state distribution	IV LSD	No change	Not associated with PsiFx	Not associated with PsiFx
LEiDA state Markov Rate	IV LSD	Not reported	Not associated with PsiFx	Weak negative association with all PsiFx
Edge-wise DCC distribution	Oral Psi*	No persisting change	Moderate-strong association with all PsiFx all networks except within motor cortex	Weak-strong association with all PsiFx in most networks
Dynamic Activity				
Multi-scale sample entropy	IV LSD	Increased at scales 1 2 and 3. Decreased at scale 5	Weak-moderate association with all PsiFx in several networks. Positive at scale 1, negative at scale 5	Weak-moderate association with all PsiFx in several networks. Positive at scale 1
BOLD complexity (spatial)	IV Psi & IV LSD	Increased (LSD) No change (psilocybin)	Not associated with PsiFx	Not associated with PsiFx
BOLD complexity (temporal)	IV Psi & IV LSD	Not reported	Weak association with SDI and Occ but not PPL	Not associated with PsiFx

**investigates persisting effects at 1 week and 1 month post-psilocybin administration*
† at thresholds producing a mean degree of 22-38
‡ at thresholds producing a mean degree of 31-38

Table 1: Summary of entropy quantification methods, previous findings, and findings reported within this manuscript. For the "Original findings" and "Our findings" columns, grey cells describe no association of effect, light grey refers to no reporting of acute effects on brain entropy, yellow describes marginal effects, and green statistically significant effects. For a more in-depth evaluation of our findings please see supplementary tables 1 and 2.

Discussion

Overview

Recent studies have reported acute psychedelic effects on functional brain entropy, but to date none of these metrics have been evaluated in an independent sample. In this study we evaluated 13 previously reported entropy metrics in a novel sample of 28 healthy participants scanned with BOLD fMRI before and several times after psilocybin with concomitant measurements of subjective drug intensity and plasma psilocin level. We observed statistically significant psilocybin effects that echoed previous reports for only two brain entropy metrics: path-length distribution, wherein we replicate increased entropy at previously reported thresholds; and sample entropy, wherein we replicate a previously observed increase in entropy at short scales and decrease at long scales. We observed a strong positive relation between psilocybin effects and brain entropy measured by Dynamic Conditional Correlation analyses that has not been previously reported. Two Lempel-Ziv complexity metrics showed some evidence for associations with psilocybin effects. For 8 of 13 brain entropy metrics previously reported, we did not observe a significant association with psilocybin measures and we see limited correlation between entropy metrics. These mixed findings underscore the importance of corroborating outcomes in independent datasets. Although we observe some evidence supporting the entropic brain hypothesis, these variable findings underscore the broadness of this theory and the need to more clearly establish which brain entropy metrics of functional brain imaging signals are acutely affected by psychedelics.

Path-length Distribution

We report a significant positive association between the Shannon entropy of the distribution of path lengths across the whole brain as previously reported by Viol and colleagues [34] and all three psilocybin metrics evaluated: PPL, Occ_{2A}, and SDI. We observed statistically significant associations at a range of correlation coefficient thresholds that produce graphs with a mean degree from 22 to 38, Viol and colleagues reported significant differences between conditions at thresholds producing mean degrees from 24 to 35. Characteristic path length is a description of the number of edges that must be traversed to get from any one brain region to another, a putative measure of capacity for information flow. Our results suggest that one of the effects of psilocybin on the brain can be described as a broadening of the histogram of path lengths across region-to-region connections in the brain. Notably, this does not imply that the average path length is shorter or longer, only that there is a wider distribution of these across the whole brain i.e., it is more equally likely that the path-length between any two nodes is 1, 2 or 3 instead of being more likely to be one of these. Our convergent results are encouraging considering that the previously reported dataset used a different drug (ayahuasca, which contains MAOIs as well as the psychedelic N,N-dimethyltryptamine) and different imaging parameters, suggesting robustness of the metric. This association with PsiFx was relatively robust to pre-processing strategies, though did appear sensitive to scanning parameters between the two explored in this study. Thus, path-length entropy may be a useful candidate biomarker of neural psychedelic effects, though associations were weak-moderate and interpretation is not straightforward. We are not aware of other studies evaluating the entropy of path-length distribution so comparison to other drugs or psychiatric conditions are not yet possible and should be evaluated in future studies.

Dynamic Conditional Correlation Distribution

We observed a statistically significant positive relation between psilocybin effects and Dynamic Conditional Correlation (DCC) Distribution for all within or between network relations except within the motor network. DCC distribution is a measure of the width of the distribution of instantaneous connectivity values for any region-region edge across each scan. The previous study found no change in DCC distribution at one-week and one-month post administration [36] and importantly did not evaluate acute effects during psilocybin. We observed moderate to strong correlations with psilocybin effects (i.e., Pearson's rho with PPL > 0.7 for three edges, all including DMN (DMN-DMN, DMN-Frontoparietal, DMN-Medial Frontal), and Pearson's rho > 0.5 for 28/36 network edges). The strength of these associations is remarkable, perhaps as large as any previously reported fMRI effect of psychedelic action, suggesting that DCC distribution may be a strong candidate neural correlate of acute psychedelic effects and among the strongest correlations observed in pharmaco-fMRI. Our results suggest that psilocybin increases the variability of connectivity between regions across time across almost all region-region pairs, which are summarised into networks. Furthermore, this association was robust to most pre-processing strategies and was similar across the two scanning parameters applied in this study. As above, we are not aware of other pharmaco-fMRI studies evaluating DCC distribution. Notwithstanding, the sheer magnitude of the observed associations suggests DCC distribution may be a sensitive marker for acute psychedelic effects on the brain and so we encourage independent replication.

Multi-scale Sample Entropy

We observed a significant positive relation between psilocybin effects and scale-1 sample entropy (i.e., temporal resolution = 2-seconds) in seven out of 17 brain networks. Conversely, we observed a significant negative relation between scale 5 sample entropy (temporal resolution = 10-seconds) in 14 out of 17 networks. This association at short-scale was somewhat robust to pre-processing pipelines and at all scales consistent across scanning parameters. Multi-scale sample entropy measures the irregularity of a signal over its entire length. Increased sample entropy in most networks at scale-1 and decreased sample entropy at scale-5 align in both cases with the original observation [29]. Unfortunately, we were unable to align the previously reported network labels with available versions of the atlas; thus, it is hard to resolve the spatial overlap between studies. fMRI-measured multi-scale sample entropy has been shown to be increased in the default-mode, visual, motor and lateral-prefrontal networks following caffeine [40] and decreased at scale 1 during sleep [37], although certain parameters used in their calculations were different to those employed here. As such, it is possible that the effects that we, and Lebedev and colleagues, observed may reflect differences in wakefulness and may thus be non-specific to psychedelic effects. Positive symptoms of schizophrenia have been positively associated with sample entropy at scales 1 and 2, and negatively associated in certain brain regions at scales 3, 4, and 5 [45]. This is consistent with our observations and is also phenomenologically consistent, as the high-dose psychedelic state has some overlap with some positive symptoms of schizophrenia e.g., verisimilitude, alterations in visual perception (though psychedelics do not normally produce 'true' hallucinations, i.e., sensory appearances indistinguishable from reality, as are present in schizophrenia), and sense of self. We are aware of the problematic history of psychedelic 'psychotomimetic' research and urge caution in overinterpretation of this apparent convergence [46]. Our convergent results with Lebedev and colleagues are intriguing considering that the original paper reported effects following intravenous LSD administration whereas we administered psilocybin orally. Taken

together, divergent effects on sample entropy at short and long temporal resolutions may be a candidate biomarker for psychedelic effects, if they cannot be explained by, e.g., wakefulness state.

Lempel-Ziv Complexity

Intriguingly, Lempel-Ziv complexity of two measures (meta-state complexity and temporal BOLD complexity (LZct)) were significantly positively associated with Occ_{2A} and SDI, but not PPL. LZct was significantly moderately associated with all PsiFx in the no-scrubbing and strict-scrubbing pre-processing pipelines, and meta-state complexity was significantly weak-moderately associated with at least one PsiFx in all but one pre-processing pipeline. The original study of meta-state complexity does not report a statistical analysis of intravenous LSD nor intravenous psilocybin effects, but the data are publicly available and do not support a significant effect of either drug [31]. The original study of BOLD complexity reports an increase in spatial BOLD complexity following LSD, but not psilocybin and does not report any findings pertaining to temporal BOLD complexity. We speculate that the less significant relations with PPL reflect that PPL is non-linearly related to brain 5-HT2A receptor occupancy, which is ultimately responsible for the neural effects of psychedelics [2]. Therefore, PPL may be a less precise metric of acute psychedelic effects on brain function. One MEG and four EEG studies have reported increased LZc following psychedelic administration [47–51], providing convergence for its utility as a marker of psychedelic effects, however one reports increases in LZct in the absence of subjective drug effects, indicating a potential epiphenomenon. Across previous studies analysing regional timeseries, there is inconsistency in the quantification of LZc in the temporal (LZct) and spatial (LZcs) domain. Our borderline statistically significant associations were observed for LZct only. It is our perspective that LZct is more sensible and should be used in future studies as it preserves region-specific temporal information, whereas LZcs is sensitive to arbitrary region order.

Null Findings

We did not observe a significant association between 8 of the 13 brain entropy metrics considered here (Table 1). Of these seven metrics, the original studies reported either increased entropy following psychedelic drug administration [19,27,28,35], no effect [30], or did not formally evaluate the effect of psychedelic drug administration [26,33] (Table 1, Supplementary Table S1). Our observed entropy estimates for hippocampal-ACC motif entropy are markedly different from those previously reported [28]. We are concerned that the originally reported values are not mathematically possible, see the Supplementary Text and Supplementary Figure S3 for a detailed consideration. Although our null findings with respect to these metrics does not establish that they have no relation to acute psychedelic drug effects, they imply a smaller relation that limits their utility as biomarkers of acute psychedelic effects. The discrepancy between our observations and those reported previously underscores the need to replicate or corroborate findings in independent cohorts to validate initial reports.

Our inability to replicate previous findings may be due to greater statistical power and different statistical models i.e., linear regression with PsiFx. Incongruence may also be attributed to differences in data collection. All previous studies reporting acute effects on brain entropy administered either 2mg of intravenous psilocybin, 75µg of intravenous LSD or 96-160mg of oral DMT with harmine, yet we administer 0.2-0.3mg/kg oral psilocybin, though the acute effect appear similar, we cannot rule out differences due to drug or route of administration. However, if entropic brain effects are not consistent

across drugs this would indicate that these metrics are not useful neural correlates of the psychedelic experience. We encourage all future fMRI studies evaluating psychedelic effects on brain function to measure subjective drug intensity at time of scanning and to collect plasma samples for quantification of plasma drug levels as described in the psychedelic fMRI consensus paper [16].

Inter-correlation Between Entropy Metrics

Despite the large set of brain entropy metrics that have been reported previously, no studies have considered whether these measures are inter-correlated. We observed positive associations between path-length and degree distribution, which are based on the same graph-theory representation of connectivity, and between LZcs and LZct which are conceptually very much related. Notably, we observed four pairs of brain entropy metrics that were significantly negatively correlated. This highlights the importance of specificity in describing "brain entropy". Many of these metrics represent distinctly different constructs, their individual meaning and collective representation of psychedelic effects is muddied by superficially considering them all metrics of "brain entropy". Future studies should be cognisant of this variable relation in considering whether findings are consistent or convergent across studies.

Alternative Neuroimaging Techniques

Although we focus here on fMRI quantifications of entropy, it is worth noting that psychedelic effects on brain entropy, specifically LZc, have been applied to five original MEG and EEG datasets, over eight papers [47–54]. The entropy measures applied in these studies leverage the high temporal sampling rate that is not clearly applicable to temporally slower fMRI and were not evaluated here. Further, the methods capture different aspects of physiological response to psychedelics. Future work evaluating psychedelic effects on brain entropy using multimodal neuroimaging and evaluating relations between alternative quantifications of brain-entropy will contribute meaningfully to the field.

Limitations

Our study is not without its limitations. Brain imaging data were acquired on two different MRI scanners with different sequences (e.g., different TRs) requiring temporal downsampling of some data to match the other. However, each participant was scanned on only one scanner, enabling us to map within-subject changes onto psilocybin effects independent of scanner differences. Our study did not include a placebo condition, but we did acquire a pre-drug scan with which we estimated brain entropy metrics in the absence of psilocybin effects. Due to the large within-subject variability in fMRI outcomes in participants scanned several days apart, pre-drug vs post-drug scans performed on the same day may be superior to placebo scans performed weeks apart for evaluating drug effects because it limits this within-subject variance component [55]. PPL and SDI were associated with increased motion in the scanner, see Supplementary Figure S4; although we included an estimate of motion as a covariate in our models, employed scrubbing, motion correction and denoising strategies, and show that motion was not positively associated with any whole-brain entropy metrics, we cannot rule out that motion confounds our reported effects. It has been reported in many groups that head motion is increased following psychedelic drug administration so this is not a limitation unique to our data [48]. Most fMRI scans were 10 minutes long, though some were only five. This may not be long enough to derive stable estimates of brain entropy metrics, e.g., previous studies have

recommended >13 minutes for single-echo fMRI [56]. Future studies, e.g., using openly available data with longer scan durations, could inform recommended scan durations to establish stable brain entropy estimates or other methods that improve signal quality, e.g., multi-echo fMRI [57]. Approximately half of the scans analysed herein utilised a multi-band acceleration protocol that may negatively affect signal-to-noise [58], though these effects may be less pronounced for task-free imaging as performed here [59]. We corrected for estimated physiological noise using aCompCor but did not statistically model physiological effects such as changes in respiration, heart rate, or vasoconstriction which are affected by psilocybin and may have confounded our findings [60,61]. Our statistical models assume a close temporal relation between brain entropy and PsiFx (measured adjacent to scans), thus, if changes in brain entropy occur after PsiFx, they would not be well captured.

Pre-processing

A prevailing challenge in fMRI research is how best to handle the enormous flexibility in data pre-processing [62]. Here we explored this space by evaluating brain entropy metrics across a set of pre-processing strategies. Most of our results were robust to using the original and common atlases, indicating robustness to parcellation choice. We also considered six different denoising strategies. The associations with PsiFx of some metrics (DCC distribution, Sample Entropy (scale 1), Meta-state complexity and Path-length distribution) were robust to most pre-processing strategies, whereas some were sensitive to pre-processing strategy, e.g., temporal BOLD complexity (LZct). For those metrics which remained significantly associated with PsiFx across pipelines, the strength of some associations varied across pipelines. Notably, the removing the low-pass filter and applying a relatively narrow bandpass filter both substantively affected the statistical relations between PsiFx and brain entropy metrics. This is consistent with previous reports that pre-processing decisions can influence observed effects on fMRI outcome measures[62], which underscores the need for future studies in large, normative datasets probing brain entropy metric characteristics in the context of this pre-processing multiverse. This is all the more relevant to advance their predictive or prognostic utility in clinical cohorts.

We provide a public MATLAB-toolbox, the Copenhagen Brain Entropy toolbox (CopBET https://github.com/anders-s-olsen/CopBET), containing functions to evaluate each of the entropy metrics evaluated here, allowing future studies to determine how these entropy metrics are affected by the multitude of possible fMRI pre-processing pipelines. For the purposes of this manuscript, we show that our pre-processing pipeline was very similar to all previously applied in this space (See Supplementary Table S7) and thus believe that our results are directly comparable with previously reported findings. We have shown that one of our findings was more strongly supported using a multi-band sequence (path-length distribution) and another when not using multi-band (Long-scale Sample Entropy). Further work may therefore also wish to apply CopBET to data collected using a range of scanning sequences to evaluate the effect of scanning parameters such as multi-band acceleration or multi-echo recording. However, given the enormous number of possible parameter choices and the unsupervised nature of the problem, interpretation of results from such an analysis remains a challenge [62].

Conclusion

In conclusion, we observed acute effects of psilocybin on 3 of 13 previously reported brain entropy metrics. We report novel evidence for a strong association effect on DCC distribution entropy, implicating it as a potential biomarker of acute psychedelic effects. We also present convergent evidence for weak associations with increases in path-length distribution entropy. In addition, two Lempel Ziv complexity measures showed marginal associations with psilocybin measures. We did not observe significant associations for 8 of 13 metrics evaluated, suggesting nuanced support for the popular theory that psychedelics acutely increase brain entropy. Our observations implicate potential brain biomarkers of acute psychedelic effects and emphasise the need for both transparency in reporting brain entropy metrics and corroborating previously reported findings in independent datasets.

Methods

Twenty-eight healthy volunteers participated in the study (10 female, mean age ± SD : 33 ± 8) and were recruited from a database of individuals interested in participating in a study involving psychedelics. A detailed description of the study design can be found in the Supplementary Text and has been reported previously [64]. The study protocol was approved by the ethics committee of the capital region of Copenhagen (H-16026898) and the Danish Medicines Agency (EudraCT no.: 2016-004000-61). The study was registered at clincaltrials.gov (NCT03289949). Data presented here were collected between 2018 and 2021. A subset of the functional brain imaging data presented here has been included in different studies reported previously [64,65]. Details of recruitment, procedures during the psilocybin session, ethical approvals, MRI acquisition and quality control, are described in the Supplementary Text. Analyses were pre-registered on the 3rd of August 2022 (https://aspredicted.org//bw8y7.pdf). Some analyses that met our inclusion criteria (i.e., fMRI studies investigating entropy changes pertaining to psychedelics) were identified after pre-registration and were added. No statistical methods were used to pre-determine sample sizes but our sample sizes are larger than all previous publications (see Figure 1).

Data Collection

After obtaining written informed consent and screening for neurological, somatic and psychiatric illness, participants completed a single-blind, cross-over study design wherein participants received a single 0.2-0.3 mg/kg dose of psilocybin (mean ± SD dose: 19.7 ± 3.6 mg, administered in units of 3 mg capsules) or 20 mg of ketanserin. Data from ketanserin scans are outside the scope of the current evaluation and not presented here. After drug administration, participants completed MRI scan sessions including resting-state fMRI (see Supplementary Text for details) approximately 40, 80, 130, and 300 minutes after administration. Following each scan, participants were asked, "On a scale from 0 to 10 how intense is your experience right now" to measure SDI and a venous blood-draw used to quantify PPL (see Supplementary Text for details). After each resting-state fMRI scan, participants were asked if they had fallen asleep (no participants reported doing so). Occ_{2A}, i.e., occupancy of psilocybin at the 5-HT2A receptor is closely related to PPL and SDI [2]. Here we applied the previously reported parameter estimates relating PPL to occupancy based on the Hill-Langmuir equation: $Occ_{2A} = \frac{Occ_{max} \times C_p}{EC_{50} + C_p}$ where Occ_{max} refers to the maximum measurable occupancy, C_p refers to the measured concentration of the ligand in plasma (i.e., PPL), and EC_{50} refers to the concentration in plasma at which occupancy is equal to 50% of Occ_{max} (fixed parameters used to compute Occ_{2A}: EC_{50} = 1.95 µg/L and Occ_{max} = 76.6%).

Pre-processing

Pre-processing and denoising was uniform across all entropy metrics despite differences in the pipelines of the original publications. Our pipeline included slice-timing correction (where applicable), unwarping, realignment, co-registration of structural scans to functional data, segmentation, normalisation, and smoothing. Two MR-scanners were used to acquire the data, and some functional data were temporally downsampled so that the sampling frequency was consistent across scan sessions. Denoising in CONN [66] included linear detrending, aCompCor [67], 12-motion (three translations, three rotations and their first derivatives) and artefact-flagged volume regression (z > 4 SDs or motion > 2 mm using ART), band-pass

filtering (0.008-0.09 Hz) and parcellation. Cerebellar ROIs were removed from included atlases as they were not consistently within the field of view. See Supplementary Text for more details.

Entropy of Static Connectivity

Four studies evaluated the entropy of static connectivity given by the matrix of Pearson correlation coefficients, **R**, computed from N-regional time-series data [27,33–35], N being the number of ROIs in the atlas used by the study.

Out-network Connectivity Distribution

Following a graph-theory framework, ROIs from the 200-region Craddock-atlas [68] were partitioned into "networks" using the Louvain modularity algorithm applied to the average connectivity matrix across scan sessions [69]. The "Out-network Connectivity", referred to as "diversity coefficient" in the original publication and "Brain Connectivity Toolbox" [27,70], of an ROI was calculated for each scan session as the Shannon entropy of the distribution of connectivity estimates between a given ROI and the set of ROIs assigned to a different network.

Degree Distribution

Degree refers to the number of non-zero elements in any given row of a thresholded matrix. ROI-specific degrees are computed based on **R**, the Pearson correlation matrix between ROIs, with N=105 using the Harvard-Oxford-105 atlas [71]. Both this analysis and Path-length distribution use the absolute correlation values. The thresholding for this analysis occurred in two steps. In the first step, any correlation for which the corresponding p-value was above 0.05 was set to 0. In the second step the goal is to reach a pre-specified mean degree across rows. In order to achieve this, a threshold below which all absolute values are set to 0 is gradually increased until the mean number of non-zero elements is at the desired level. Here we applied a scan-specific threshold that produced a mean degree of 27 because this was the threshold that produced the largest effect in the original publication [35]. This means that each scan may have a different absolute threshold value, but identical mean degree. The final entropy quantification is simply the Shannon entropy of the distribution of degrees across ROIs. We also calculated entropy for mean degrees of 1 up to the point at which for any given scan session an increase in absolute threshold did not produce an increase in mean degree, i.e., 48. This also applies to the path-length entropy described below.

Path-length Distribution

Again using absolute correlation values, the matrix was thresholded using only the mean-degree criteria and not the p-value threshold. The matrix was then binarised, setting all non-zero elements to 1. The "shortest path length" was then computed as the fewest edges one must traverse to go from one node to another. The Shannon entropy of the distribution of path lengths from each node to all other nodes was then calculated [34]. Path-length distribution was evaluated for correlation coefficient thresholds up to a mean degree of 53.

Von Neumann Entropy

Entropy of the Pearson correlation matrix, **R**, derived for the Harvard-Oxford-105 atlas, was calculated through the von Neumann entropy: $S(\boldsymbol{\rho}) = -\sum_{i=1}^{N} \lambda_i \, log \, \lambda_i$, where λ are the eigenvalues of the scaled correlation matrix $\boldsymbol{\rho}=\mathbf{R}/N$. The von Neumann entropy may also be defined as $S(\boldsymbol{\rho}) = -tr(\boldsymbol{\rho} log \boldsymbol{\rho})$, where log represents the matrix logarithm [33].

Entropy of Dynamic Connectivity

Intra-network Synchrony Distribution

Nine brain networks were defined according to a previous study [72]: auditory, dorsal attention, default mode, left and right frontoparietal, motor, salience, visual 1 and visual 2. For a given network, for a given time point, the variance across voxels within the network was evaluated. The Shannon entropy was then calculated on the histogram of the variance estimates over time [19].

Motif-connectivity Distribution

Dynamic functional brain connectivity was evaluated in four regions (10mm diameter spheres) located at bilateral hippocampi, MNI coordinates: right: (26, -21, -16), left: (-34, -22, -16), and anterior cingulate cortices, right: (4, 35, 18), left: (-2, 23 ,28) using a non-overlapping sliding window approach with varying window lengths (15-150s). In each window, the partial correlation coefficient and corresponding p-value was calculated for every region pair, controlling for the remaining regions and the motion framewise displacement time-series. These time-series were standardised before windowing. The 4 x 4 partial correlation matrix was binarised for every window, according to a corrected significance threshold p=0.0083 (i.e., 0.05/6, where 6 is the number of region pairs). A probability distribution of the frequency of each of the 64 possible graph structures was established and the Shannon entropy was calculated [28].

LEiDA-state Markov-rate

Notably, this entropy metric was not applied to evaluate psychedelic effects in the original paper. Rather, the authors provided a computational framework wherein parameters were learned by optimising this entropy measure. For each scan session, Leading Eigenvector Dynamics Analysis (LEiDA) [73] was applied to the time-series of 90 AAL atlas regions [74]. The phase series was computed using the Hilbert transform and, for each time point, a phase coherence matrix was estimated based on the cosine of the difference between pairwise instantaneous phases. The phase coherence matrices were decomposed using the eigenvalue decomposition and the first eigenvector was retained for every time point. The set of eigenvectors was clustered using *K*-means with $K = 3$ states. Subsequently, the transition probability matrix was computed for each scan session. The entropy rate of the transition matrix, $P(i,j)$, for each state, i, was calculated as $Si = -p(i)\sum_{j=1}^{K} P(i,j) log P(i,j)$.where, p is the leading eigenvector of P. The final entropy measure is given as $S = \sum_{j=1}^{K} S_i \, / log_2(K)$ [26].

Dynamic Conditional Correlation Distribution

Regional time-series were evaluated for each of the regions described in the Shen 268 region atlas [75]. Windowless framewise correlation coefficients were calculated for all edges using the Dynamic Conditional Correlation (DCC) toolbox [76]. Subsequently, the probability distribution over each ROI-to-ROI DCC time-series was established, and the Shannon entropy was calculated. Each ROI was assigned to one of eight networks: default mode, fronto-parietal, medial-frontal, motor, subcortical-cerebellar, visual association, visual 1, and visual 2. Each ROI-to-ROI pair was assigned to its respective network-to-network association (e.g., motor-to-motor, default mode-to-motor) and the mean entropy of each network-to-network association was calculated. Although the original publication applies bin-width correction, they do not report an effect of bin width and we report findings using MATLAB's *histcounts* function, which automatically calculates bin-width [36]. Thus, we did not implement bin-width correction.

Meta-state Complexity

Regional time-series were evaluated for each of the regions described in the Lausanne 463 region atlas [77]. BOLD time-series across all scan sessions were clustered using *K*-means into $K = 4$ states using the Pearson correlation distance metric. The clustering procedure was repeated 200 times with random initialisations and the best repeat in terms of *K*-means loss was extracted. The four states were grouped into two meta-states because the clustering procedure typically produces sign-symmetric states. Each volume was assigned to meta-state 0 or 1 and the Lempel-Ziv complexity (LZ76 exhaustive algorithm) of this binary sequence was calculated [31].

Integration/Segregation-state Distribution

Regional time-series were evaluated for each region described in the Schaefer 200 region atlas [44], augmented with 32 subcortical regions from the Tian atlas [43]. A sliding-window correlation analysis was performed using a window defined by convolving a rectangular window of size 44 seconds with a temporal Gaussian kernel (FWHM = 3s). The correlation matrix was established for each window (stride of 1), and the Louvain modularity algorithm [69] was applied to estimate the module degree z-score and participation coefficient for each region. The Louvain modularity algorithm was repeated 100 times to ensure an optimal assignment. *K*-means clustering with $K = 2$ states was applied to a cartographic profile, i.e., a two-dimensional unnormalised histogram of these measures, using the correlation distance and 500 replications. The Shannon entropy was computed on the probability distribution of state occurrences [30].

Entropy of Regional Dynamics

Multi-scale Sample Entropy

Networks were defined using the Yeo 17-network atlas [78]. Sample entropy is defined as the negative logarithm of the conditional probability that if two vectors with length m (set to 2) are dissimilar below a threshold distance r (set as 0.3), then vector pairs with length $m + 1$ will also have distance below the threshold [21]. Scales 1-5 were evaluated for each network, meaning that each time-series was split into non-overlapping windows of length (scale) s volumes and the means of each window were concatenated to form a condensed time-series upon which sample entropy was calculated [29].

BOLD Complexity

Regional time-series were evaluated for each of the regions described in the Schaefer 1000 region atlas [44]. BOLD time-series for each ROI were first Hilbert-transformed. The amplitude of the Hilbert series was then binarised around the mean amplitude for that region, i.e., assigned as "1" if greater than the mean and "0" if less. These binarised time-series were combined into an $T \times N$ matrix, where $N = 1000$ is the number of regions and T and is the number of time points.This matrix was collapsed into a single vector to compute 1) the Lempel-Ziv complexity over time (LZct, LZ78 algorithm) wherein regional time-series were concatenated or 2) Lempel-Ziv complexity over space (LZcs) wherein time-adjacent "region series" were concatenated. LZct represents a calculation of the temporal entropy of each ROI, whereas LZcs represents a calculation of the spatial entropy at each timepoint. The original publication [32] reported only LZcs, but LZct is also described in [47] whom Varley and colleagues reference as the source of their methods.

Statistical Model

Effects of psilocybin on brain entropy metrics were estimated using a linear mixed effects model with relevant R packages, i.e., *predictmeans* (v1.0.6), *lme4* (v1.1.30), *nlme* (v3.1.157), *lmerTest* (v3.1.3) and *LMMstar* (v0.7.6). We regressed each metric against each of the three measures (PPL, SDI, or Occ_{2A}) separately with a subject-specific random intercept and adjusting for motion, age, sex, and scanner. A test statistic for the association between metric and measure was obtained using the Wald statistic. To ensure adequate control of the family-wise error rate (FWER) across regions within each of the 13 metrics, (e.g., 17 networks for one time scale of multi-scale sample entropy), we calculate p_{FWER} adjusted using the maxT test method [42] in a permutation framework similar to [79], employing 10000 permutations. As such, if observed data superseded all permutations, the p-value is reported as $p < 0.0001$. "Motion" reflects the framewise displacement computed using the Artifact Detection Toolbox (ART) (see Supplementary Text) and "scanner" controls for MR scanner, of which there were two. We do not adjust p-values across metrics, nor across SDI, PPL and Occ_{2A}; unadjusted p-values are reported for non-regional metrics as p_{perm}. We defined findings as statistically significant if they were associated with all three psilocybin effects, SDI, PPL and Occ_{2A} (collectively summarised "PsiFx") at $p_{perm} < 0.05$ for non-regional metrics or $p_{FWER} < 0.05$ for regional metrics. Effect sizes are reported as Pearson's correlation coefficient between the partial residuals of the entropy metrics (adjusted for covariates using the mixed-model described above) and each of PsiFx. The strength of Pearson's correlation coefficients for significant associations are described as "weak" (≤0.3), "moderate" (>0.3 and ≤0.6), or "strong" (>0.6) as previously defined [80].

Moderating Effect of Scanner

Our data were collected on one of two MRI scanners. In order to investigate whether scanner choice had an impact on the estimated relation between PPL and entropy moderating effects of scanner were explored in separate models that included the scanner-x-PPL interaction as an additional covariate.

Correlation Between Metrics

Simple Pearson correlation coefficients were calculated between each whole-brain entropy metric pair as well as with motion. Of the two graph theory metrics requiring thresholding, the threshold producing a

mean degree of 27 was used. For the motif-connectivity distribution, 15 and 100 second windows were selected to represent fast and slow dynamics, respectively. P-values were adjusted using Bonferroni correction [81]. All scans remaining after pre-processing were used in these analyses.

Effect of Parcellation

To explore parcellation effects on outcomes, all entropy metrics were evaluated using the Schaefer 100 region atlas with 16 subcortical regions from the Tian atlas [43,44]. For metrics using network definitions, the Yeo 7-network atlas was applied as a common atlas.

Effect of Pre-processing Pipelines

To explore the effect of pre-processing decisions on the associations between PsiFx and brain entropy metrics, analyses were repeated for six additional pre-processing pipelines. Each pre-processing pipeline was run on the data parcellated as described in the section “Effect of parcellation” i.e., 116 ROIs assigned to seven networks. Each pipeline changed one variable from the “reference” pipeline. These were as follows: 1) adding global signal regression, 2) removing the low-pass 0.09 Hz filter (i.e., not removing high-frequency signal), 3) expanding the 12-motion regressors to include squares of the derivatives (i.e., Volterra expansion), 4) not regressing out flagged volumes 5) regressing flagged volumes with a stricter threshold (z >3 or motion>0.5mm), (6) applying a narrower bandpass filter (0.03-0.07 Hz).

Code and Data Availability

We shared relevant analysis scripts with original authors, hoping to ensure as much as possible that our computations aligned with original reports; we are thankful for the feedback we received. All functions used to derive entropy estimates from pre-processed data have been compiled into the "Copenhagen Brain Entropy Toolbox" (CopBET), a Matlab-based toolbox that can be found here: https://github.com/anders-s-olsen/CopBET. The permutation testing code is also available here. Code for other statistical analyses and figures can be made available upon request. The data that support the findings of this study are available from the corresponding author upon request to the CIMBI database [82].

Acknowledgements

A sincere thank you to Andrea Luppi, Enzo Tagliazucchi, Alexander Lebedev, Manoj Doss, Thomas Varley, and Parker Singleton for their advice and feedback regarding their entropy metrics, including advice from Drs Doss and Varley to not use their entropy metrics, as they no longer believed them to be valid, which we appreciate, but disregarded.

Conflict Statement

DEWM salary is supported by an unrestricted grant from COMPASS Pathways who have no involvement in the preparation or conception of this manuscript or related data collection. MKM has received an honorarium as a speaker for H. Lundbeck. GMK has served as a consultant for Sanos, Gilgamesh, Onsero,

Pangea, Abbvie, PureHealthTech, and has received honoraria as speaker for H. Lundbeck and Sage Therapeutics.

Author Contributions

DEWM conceptualised the manuscript idea, collected data, performed analyses, and wrote the manuscript. ASO conceptualised the manuscript idea, performed analyses, prepared the CopBET, and wrote the manuscript. BO supported statistical analyses and related software. DSS facilitated, supervised, and performed data collection. SA performed data collection. MKM conceptualised the original study, and facilitated and performed data collection. GMK obtained core study funding, conceptualised the original study, and provided feedback on the project. PMF conceptualised the original study, facilitated data collection, and supervised data analysis and manuscript writing. All co-authors reviewed the manuscript, provided feedback, and approved the final version.

References

1. Becker, A. M. *et al.* Acute Effects of Psilocybin After Escitalopram or Placebo Pretreatment in a Randomized, Double-Blind, Placebo-Controlled, Crossover Study in Healthy Subjects. *Clin. Pharmacol. Ther.* **111**, 886–895 (2022).
2. Madsen, M. K. *et al.* Psychedelic effects of psilocybin correlate with serotonin 2A receptor occupancy and plasma psilocin levels. *Neuropsychopharmacology* **44**, 1328–1334 (2019).
3. Nichols, D. E. Psychedelics. *Pharmacol. Rev.* (2016) doi:10.1124/pr.115.011478.
4. Wallach, J. *et al.* Identification of 5-HT2A receptor signaling pathways associated with psychedelic potential. *Nat. Commun.* **14**, 8221 (2023).
5. Anderson, B. T. *et al.* Psilocybin-assisted group therapy for demoralized older long-term AIDS survivor men: An open-label safety and feasibility pilot study. *EClinicalMedicine* **27**, 100538 (2020).
6. Bogenschutz, M. P. *et al.* Percentage of Heavy Drinking Days Following Psilocybin-Assisted Psychotherapy vs Placebo in the Treatment of Adult Patients With Alcohol Use Disorder. *JAMA Psychiatry* **79**, 953 (2022).
7. Carhart-Harris, R. *et al.* Trial of Psilocybin versus Escitalopram for Depression. *N. Engl. J. Med.* **384**, 1402–1411 (2021).
8. Carhart-Harris, R. L. *et al.* Psilocybin with psychological support for treatment-resistant depression: six-month follow-up. *Psychopharmacology (Berl.)* **235**, 399–408 (2018).
9. Goodwin, G. M. *et al.* Single-Dose Psilocybin for a Treatment-Resistant Episode of Major Depression. *N. Engl. J. Med.* **387**, 1637–1648 (2022).
10. Griffiths, R. R. *et al.* Psilocybin produces substantial and sustained decreases in depression and anxiety in patients with life-threatening cancer: A randomized double-blind trial. *J. Psychopharmacol. (Oxf.)* **30**, 1181–1197 (2016).
11. Holze, F., Gasser, P., Müller, F., Dolder, P. C. & Liechti, M. E. Lysergic Acid Diethylamide–Assisted Therapy in Patients With Anxiety With and Without a Life-Threatening Illness: A Randomized,

Double-Blind, Placebo-Controlled Phase II Study. *Biol. Psychiatry* (2022) doi:10.1016/j.biopsych.2022.08.025.

12. Johnson, M. W., Garcia-Romeu, A. & Griffiths, R. R. Long-term follow-up of psilocybin-facilitated smoking cessation. *Am. J. Drug Alcohol Abuse* **43**, 55–60 (2017).
13. Griffiths, R. R. *et al.* Psilocybin occasioned mystical-type experiences: Immediate and persisting dose-related effects. *Psychopharmacology (Berl.)* **218**, 649–665 (2011).
14. McCulloch, D. E.-W. *et al.* Psilocybin-Induced Mystical-Type Experiences are Related to Persisting Positive Effects: A Quantitative and Qualitative Report. *Front. Pharmacol.* **13**, 1–17 (2022).
15. Schmid, Y. & Liechti, M. E. Long-lasting subjective effects of LSD in normal subjects. *Psychopharmacology (Berl.)* **235**, 535–545 (2018).
16. McCulloch, D. E.-W. *et al.* Psychedelic resting-state neuroimaging: A review and perspective on balancing replication and novel analyses. *Neurosci. Biobehav. Rev.* **138**, 104689 (2022).
17. Doss, M. K. *et al.* Models of psychedelic drug action: modulation of cortical-subcortical circuits. *Brain* (2021) doi:10.1093/brain/awab406.
18. Carhart-Harris, R. L. The entropic brain - revisited. *Neuropharmacology* **142**, 167–178 (2018).
19. Carhart-Harris, R. L. *et al.* The entropic brain: A theory of conscious states informed by neuroimaging research with psychedelic drugs. *Front. Hum. Neurosci.* **8**, 1–22 (2014).
20. Shannon, C. E. A mathematical theory of communication. *Bell Syst. Tech. J.* **27**, 379–423 (1948).
21. Delgado-Bonal, A. & Marshak, A. Approximate Entropy and Sample Entropy: A Comprehensive Tutorial. *Entropy* **21**, 541 (2019).
22. Lempel, A. & Ziv, J. On the Complexity of Finite Sequences. *IEEE Trans. Inf. Theory* **22**, 75–81 (1976).
23. Richman, J. S. & Moorman, J. R. Physiological time-series analysis using approximate entropy and sample entropy maturity in premature infants Physiological time-series analysis using approximate entropy and sample entropy. *Am. J. Physiol. Heart Circ. Physiol.* **278**, H2039–H2049 (2000).

24. Ziv, J. & Lempel, A. Compression of individual sequences via variable-rate coding. *IEEE Trans. Inf. Theory* **24**, 530–536 (1978).
25. Rubinov, M. & Sporns, O. Complex network measures of brain connectivity: Uses and interpretations. *NeuroImage* **52**, 1059–1069 (2010).
26. Kringelbach, M. L. *et al.* Dynamic coupling of whole-brain neuronal and neurotransmitter systems. *Proc. Natl. Acad. Sci.* **117**, 9566–9576 (2020).
27. Lebedev, A. V. *et al.* Finding the self by losing the self: Neural correlates of ego-dissolution under psilocybin: Finding the Self by Losing the Self. *Hum. Brain Mapp.* **36**, 3137–3153 (2015).
28. Tagliazucchi, E., Carhart-Harris, R., Leech, R., Nutt, D. & Chialvo, D. R. Enhanced repertoire of brain dynamical states during the psychedelic experience. *Hum. Brain Mapp.* **35**, 5442–5456 (2014).
29. Lebedev, A. V. *et al.* LSD-induced entropic brain activity predicts subsequent personality change: LSD-Induced Entropic Brain Activity. *Hum. Brain Mapp.* **37**, 3203–3213 (2016).
30. Luppi, A. I. *et al.* LSD alters dynamic integration and segregation in the human brain. *NeuroImage* **227**, 117653 (2021).
31. Singleton, S. P. *et al.* Receptor-informed network control theory links LSD and psilocybin to a flattening of the brain's control energy landscape. *Nat. Commun.* **13**, 5812 (2022).
32. Varley, T. F., Carhart-Harris, R., Roseman, L., Menon, D. K. & Stamatakis, E. A. Serotonergic psychedelics LSD & psilocybin increase the fractal dimension of cortical brain activity in spatial and temporal domains. *NeuroImage* **220**, 117049 (2020).
33. Felippe, H. *et al.* The von Neumann entropy for the Pearson correlation matrix: A test of the entropic brain hypothesis. in (2021).
34. Viol, A. *et al.* Characterizing Complex Networks Using Entropy-Degree Diagrams: Unveiling Changes in Functional Brain Connectivity Induced by Ayahuasca. *Entropy 2019 Vol 21 Page 128* **21**, 128 (2019).

35. Viol, A., Palhano-Fontes, F., Onias, H., De Araujo, D. B. & Viswanathan, G. M. Shannon entropy of brain functional complex networks under the influence of the psychedelic Ayahuasca. *Sci. Rep.* **7**, 1–13 (2017).

36. Barrett, F. S., Doss, M. K., Sepeda, N. D., Pekar, J. J. & Griffiths, R. R. Emotions and brain function are altered up to one month after a single high dose of psilocybin. *Sci. Rep.* **10**, 2214 (2020).

37. Kung, Y.-C. *et al.* Cross-Scale Dynamicity of Entropy and Connectivity in the Sleeping Brain. *Brain Connect.* **12**, 835–845 (2022).

38. Maki-Marttunen, V., Diez, I., Cortes, J., Chialvo, D. & Villarreal, M. Disruption of transfer entropy and inter-hemispheric brain functional connectivity in patients with disorder of consciousness. *Front. Neuroinformatics* **7**, (2013).

39. Pappas, I., Adapa, R. M., Menon, D. K. & Stamatakis, E. A. Brain network disintegration during sedation is mediated by the complexity of sparsely connected regions. *NeuroImage* **186**, 221–233 (2019).

40. Chang, D. *et al.* Caffeine Caused a Widespread Increase of Resting Brain Entropy. *Sci. Rep.* **8**, 2700 (2018).

41. Doss, M. K. *et al.* The Acute Effects of the Atypical Dissociative Hallucinogen Salvinorin A on Functional Connectivity in the Human Brain. *Sci. Rep.* (2020) doi:10.1038/s41598-020-73216-8.

42. Westfall, P. H. & Troendle, J. F. Multiple Testing with Minimal Assumptions. *Biom. J. Biom. Z.* **50**, 745–755 (2008).

43. Tian, Y., Margulies, D. S., Breakspear, M. & Zalesky, A. Topographic organization of the human subcortex unveiled with functional connectivity gradients. *Nat. Neurosci.* (2020) doi:10.1038/s41593-020-00711-6.

44. Schaefer, A. *et al.* Local-Global Parcellation of the Human Cerebral Cortex from Intrinsic Functional Connectivity MRI. *Cereb. Cortex* (2018) doi:10.1093/cercor/bhx179.

45. Yang, A. C. *et al.* Decreased resting-state brain activity complexity in schizophrenia characterized by both increased regularity and randomness. *Hum. Brain Mapp.* **36**, 2174–2186 (2015).

801 46. Nichols, D. E. & Walter, H. The History of Psychedelics in Psychiatry. *Pharmacopsychiatry* **54**, 151–
802 166 (2021).
803 47. Schartner, M. M., Carhart-Harris, R. L., Barrett, A. B., Seth, A. K. & Muthukumaraswamy, S. D.
804 Increased spontaneous MEG signal diversity for psychoactive doses of ketamine, LSD and psilocybin.
805 *Sci. Rep.* **7**, 46421 (2017).
806 48. Timmermann, C. *et al.* Human brain effects of DMT assessed via EEG-fMRI. *Proc. Natl. Acad. Sci.*
807 **120**, e2218949120 (2023).
808 49. Timmermann, C. *et al.* Neural correlates of the DMT experience assessed with multivariate EEG. *Sci.*
809 *Rep.* **9**, 16324 (2019).
810 50. Pallavicini, C. *et al.* Neural and subjective effects of inhaled N,N-dimethyltryptamine in natural
811 settings. *J. Psychopharmacol. (Oxf.)* **35**, 406–420 (2021).
812 51. Murray, C. H. *et al.* Neural complexity is increased after low doses of LSD, but not moderate to high
813 doses of oral THC or methamphetamine. *Neuropsychopharmacology* 1–9 (2024) doi:10.1038/s41386-
814 024-01809-2.
815 52. Singleton, S. P. *et al.* Time-resolved network control analysis links reduced control energy under DMT
816 with the serotonin 2a receptor, signal diversity, and subjective experience. *BioRxiv Prepr. Serv. Biol.*
817 2023.05.11.540409 (2023) doi:10.1101/2023.05.11.540409.
818 53. Toker, D. *et al.* Consciousness is supported by near-critical slow cortical electrodynamics. *Proc. Natl.*
819 *Acad. Sci.* **119**, e2024455119 (2022).
820 54. Eckernäs, E., Timmermann, C., Carhart-Harris, R., Röshammar, D. & Ashton, M. N,N-
821 dimethyltryptamine affects electroencephalography response in a concentration-dependent manner—
822 A pharmacokinetic/pharmacodynamic analysis. *CPT Pharmacomet. Syst. Pharmacol.* **12**, 474–486
823 (2023).
824 55. Noble, S., Scheinost, D. & Constable, R. T. A decade of test-retest reliability of functional connectivity:
825 A systematic review and meta-analysis. *NeuroImage* **203**, 116157 (2019).

826 56. Birn, R. M. *et al.* The effect of scan length on the reliability of resting-state fMRI connectivity
827 estimates. *NeuroImage* **83**, 550–558 (2013).
828 57. Kundu, P. *et al.* Multi-echo fMRI: A review of applications in fMRI denoising and analysis of BOLD
829 signals. *NeuroImage* **154**, 59–80 (2017).
830 58. Risk, B. B. *et al.* Which multiband factor should you choose for your resting-state fMRI study?
831 *NeuroImage* **234**, 117965 (2021).
832 59. Demetriou, L. *et al.* A comprehensive evaluation of increasing temporal resolution with multiband-
833 accelerated protocols and effects on statistical outcome measures in fMRI. *NeuroImage* **176**, 404–416
834 (2018).
835 60. Dyer, D. C. & Gant, D. W. Vasoconstriction Produced by Hallucinogens on Isolated Human and Sheep
836 Umbilical Vasculature. *J. Pharmacol. Exp. Ther.* **184**, 366–375 (1973).
837 61. Holze, F., Becker, A. M., Kolaczynska, K. E., Duthaler, U. & Liechti, M. E. Pharmacokinetics and
838 Pharmacodynamics of Oral Psilocybin Administration in Healthy Participants. *Clin. Pharmacol. Ther.*
839 **113**, 822–831 (2023).
840 62. Carp, J. On the Plurality of (Methodological) Worlds: Estimating the Analytic Flexibility of fMRI
841 Experiments. *Front. Neurosci.* **6**, (2012).
842 63. Van Essen, D. C. *et al.* The WU-Minn Human Connectome Project: An overview. *NeuroImage* (2013)
843 doi:10.1016/j.neuroimage.2013.05.041.
844 64. Madsen, M. K. *et al.* Psilocybin-induced changes in brain network integrity and segregation correlate
845 with plasma psilocin level and psychedelic experience. *Eur. Neuropsychopharmacol.* **50**, 121–132
846 (2021).
847 65. Olsen, A. S. *et al.* Psilocybin modulation of time-varying functional connectivity is associated with
848 plasma psilocin and subjective effects. *NeuroImage* 119716 (2022)
849 doi:10.1016/J.NEUROIMAGE.2022.119716.
850 66. Whitfield-Gabrieli, S. & Nieto-Castanon, A. Conn: A Functional Connectivity Toolbox for Correlated
851 and Anticorrelated Brain Networks. *Brain Connect.* (2012) doi:10.1089/brain.2012.0073.

852 67. Behzadi, Y., Restom, K., Liau, J. & Liu, T. T. A component based noise correction method (CompCor)
853 for BOLD and perfusion based fMRI. *NeuroImage* (2007) doi:10.1016/j.neuroimage.2007.04.042.
854 68. Craddock, R. C., James, G. A., Holtzheimer, P. E., Hu, X. P. & Mayberg, H. S. A whole brain fMRI
855 atlas generated via spatially constrained spectral clustering. *Hum. Brain Mapp.* (2012)
856 doi:10.1002/hbm.21333.
857 69. Blondel, V. D., Guillaume, J.-L., Lambiotte, R. & Lefebvre, E. Fast unfolding of communities in large
858 networks. *J. Stat. Mech. Theory Exp.* **2008**, P10008 (2008).
859 70. Bullmore, E. & Sporns, O. Complex brain networks: graph theoretical analysis of structural and
860 functional systems. *Nat. Rev. Neurosci.* **10**, 186–198 (2009).
861 71. Desikan, R. S. *et al.* An automated labeling system for subdividing the human cerebral cortex on MRI
862 scans into gyral based regions of interest. *NeuroImage* (2006) doi:10.1016/j.neuroimage.2006.01.021.
863 72. Smith, S. M. *et al.* Correspondence of the brain's functional architecture during activation and rest.
864 *Proc. Natl. Acad. Sci. U. S. A.* (2009) doi:10.1073/pnas.0905267106.
865 73. Cabral, J. *et al.* Cognitive performance in healthy older adults relates to spontaneous switching between
866 states of functional connectivity during rest. *Sci. Rep.* **7**, 5135 (2017).
867 74. Tzourio-Mazoyer, N. *et al.* Automated anatomical labeling of activations in SPM using a macroscopic
868 anatomical parcellation of the MNI MRI single-subject brain. *NeuroImage* (2002)
869 doi:10.1006/nimg.2001.0978.
870 75. Shen, X., Tokoglu, F., Papademetris, X. & Constable, R. T. Groupwise whole-brain parcellation from
871 resting-state fMRI data for network node identification. *NeuroImage* (2013)
872 doi:10.1016/j.neuroimage.2013.05.081.
873 76. Lindquist, M. A., Xu, Y., Nebel, M. B. & Caffo, B. S. Evaluating Dynamic Bivariate Correlations in
874 Resting-state fMRI: A comparison study and a new approach. *NeuroImage* **101**, 531–546 (2014).
875 77. Daducci, A. *et al.* The Connectome Mapper: An Open-Source Processing Pipeline to Map
876 Connectomes with MRI. *PLOS ONE* **7**, e48121 (2012).

78. Yeo, B. T. *et al.* The organization of the human cerebral cortex estimated by intrinsic functional connectivity. *J. Neurophysiol.* (2011) doi:10.1152/jn.00338.2011.

79. Lee, O. E. & Braun, T. M. Permutation tests for random effects in linear mixed models. *Biometrics* **68**, 486–493 (2012).

80. Akoglu, H. User's guide to correlation coefficients. *Turk. J. Emerg. Med.* **18**, 91–93 (2018).

81. Haynes, W. Bonferroni Correction. in *Encyclopedia of Systems Biology* 154–154 (Springer New York, New York, NY, 2013). doi:10.1007/978-1-4419-9863-7_1213.

82. Knudsen, G. M. *et al.* The Center for Integrated Molecular Brain Imaging (Cimbi) database. *NeuroImage* **124**, 1213–1219 (2016).

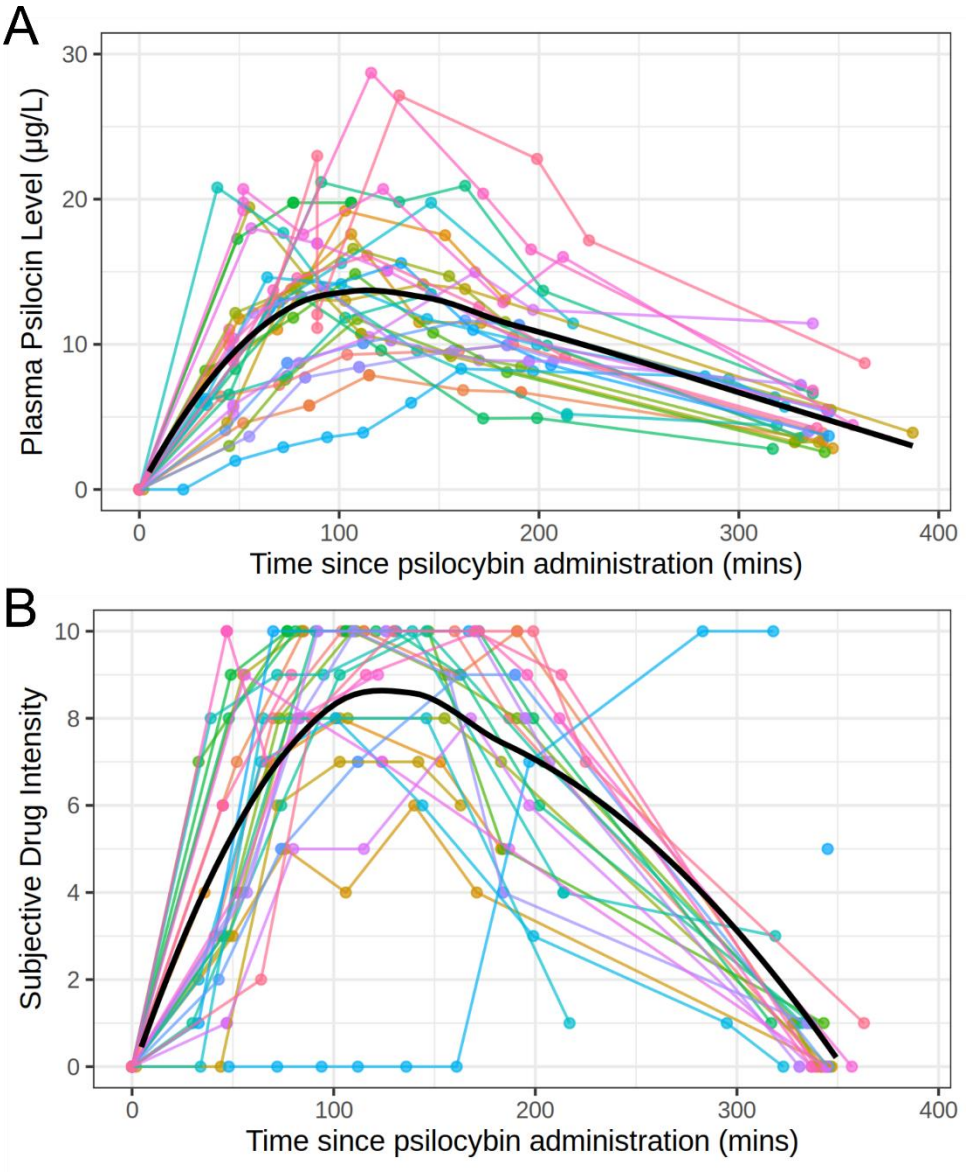

888

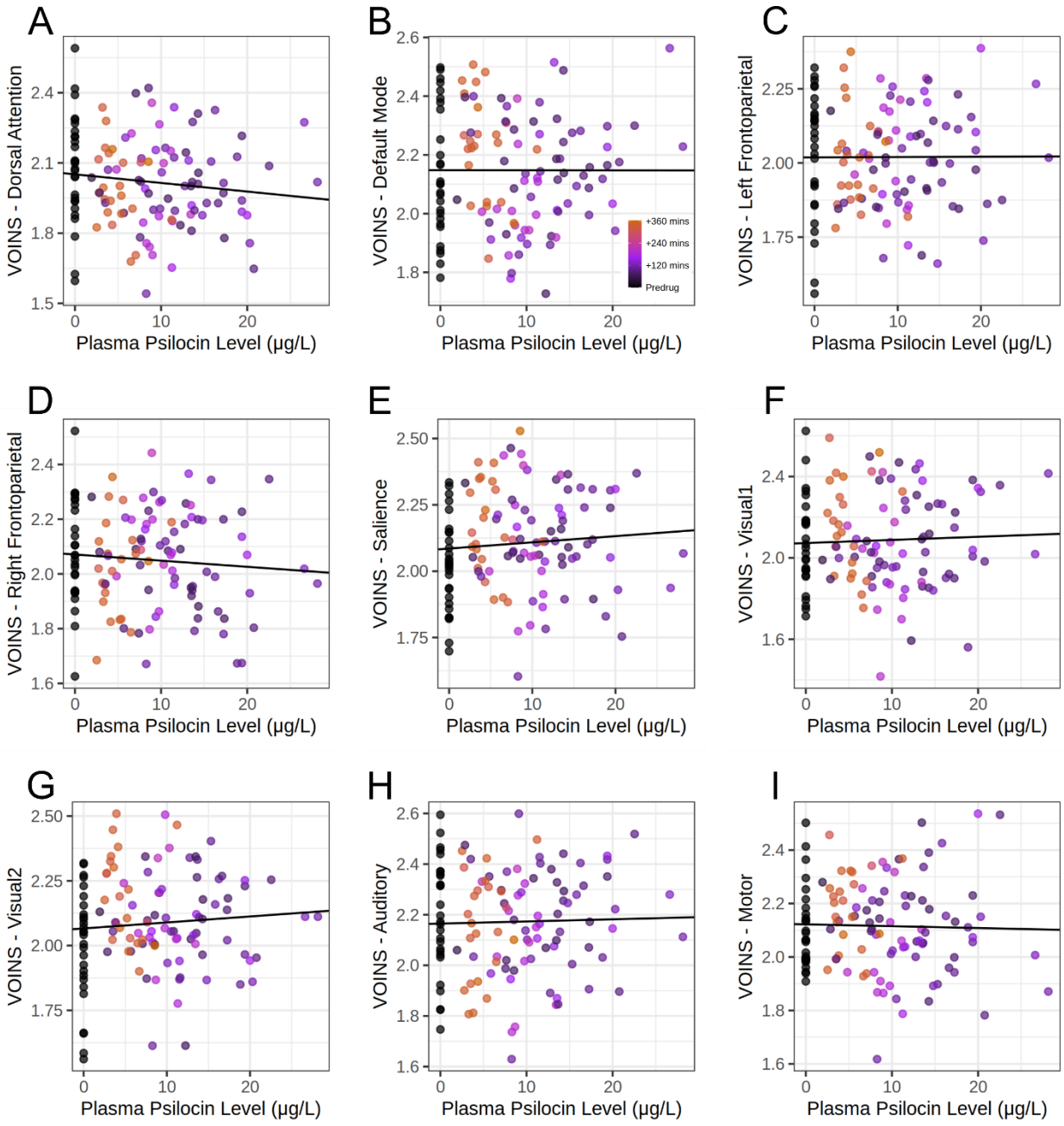

889

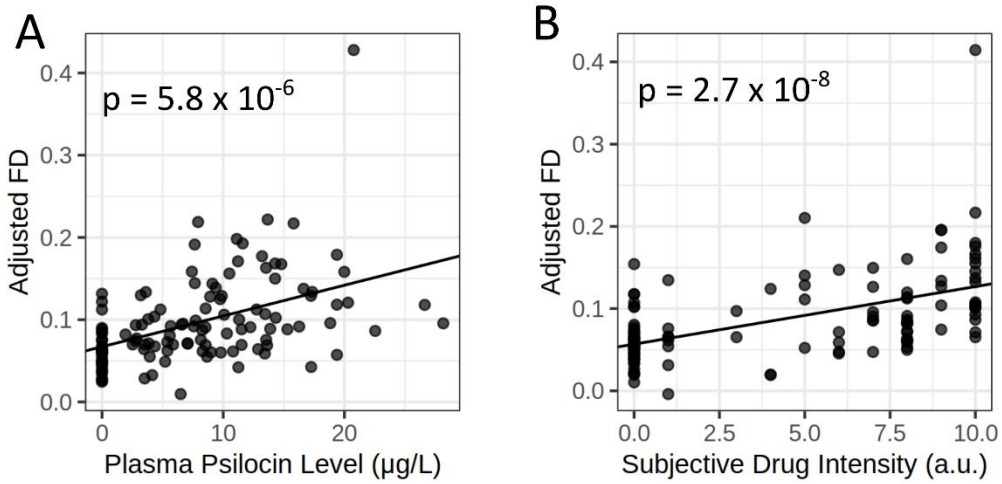

890

Entropy	Original dataset	Original findings	Our findings (original atlases)	Our findings (common atlas)
Static Connectivity				
Out-network connectivity	IV Psi	Region-specific effects	Not associated with PsiFx	Not associated with PsiFx
Degree distribution	Oral Aya	Increased	Not associated with PsiFx	Not associated with PsiFx
Path-length distribution	Oral Aya	Increased	Weak-moderate association with PsiFx†	Weak-moderate association with PsiFx‡
Von Neumann Entropy	Oral Aya	Numerically increased	Not associated with PsiFx	Not associated with PsiFx
Dynamic Connectivity				
Intra-network synchrony	IV Psi	Increased (some networks)	Not associated with PsiFx	Not associated with PsiFx
Motif-connectivity distribution	IV Psi	Increased	Not associated with PsiFx	Not atlas dependent
Meta-state complexity	IV Psi & IV LSD	No change	Weak association with SDI and Occ but not PPL	Weak association with Occ but not SDI or PPL
I/S state distribution	IV LSD	No change	Not associated with PsiFx	Not associated with PsiFx
LEiDA state Markov Rate	IV LSD	Not reported	Not associated with PsiFx	Weak negative association with all PsiFx
Edge-wise DCC distribution	Oral Psi*	No persisting change	Moderate-strong association with all PsiFx all networks except within motor cortex	Weak-strong association with all PsiFx in most networks
Dynamic Activity				
Multi-scale sample entropy	IV LSD	Increased at scales 1 2 and 3. Decreased at scale 5	Weak-moderate association with all PsiFx in several networks. Positive at scale 1, negative at scale 5	Weak-moderate association with all PsiFx in several networks. Positive at scale 1
BOLD complexity (spatial)	IV Psi & IV LSD	Increased (LSD) No change (psilocybin)	Not associated with PsiFx	Not associated with PsiFx
BOLD complexity (temporal)	IV Psi & IV LSD	Not reported	Weak association with SDI and Occ but not PPL	Not associated with PsiFx

**Investigates persisting effects at 1 week and 1 month post-psilocybin administration*

† at thresholds producing a mean degree of 22-38

‡ at thresholds producing a mean degree of 31-38